International Journal of Control, Automation and Systems 16(6) (2018) 2575-2584
http://dx.doi.org/10.1007/s12555-018-0112-z
ISSN:1598-6446 eISSN:2005-4092
http://www.springer.com/12555

Quaternion-based Robust Trajectory Tracking Control of a Quadrotor Hover System

Derek Hoffman, Muhammad Rehan, William MacKunis, and Mahmut Reyhanoglu*

Abstract: This paper presents a robust nonlinear output feedback control method that achieves three degree of freedom (3-DOF) attitude trajectory tracking of a hover system test bed. The proposed control method formally incorporates dynamic model uncertainty in addition to test bed voltage constraints. To reduce the computational requirement in the closed-loop system, constant feedforward estimates of the input-multiplicative parametric uncertainty are utilized in lieu of adaptive parameter estimates. To eliminate the need for angular rate measurements, the control design employs a bank of dynamic filters, which operates as a velocity estimator in the closed-loop system. A rigorous error system development and Lyapunov-based stability analysis are presented to prove asymptotic 3-DOF attitude trajectory tracking control. Computer simulation and experimental results are also included to illustrate the performance of the attitude control method using the Quanser 3-DOF hover system test bed.

Keywords: Output feedback, quadrotor, quaternion, robust, tracking.

1. INTRODUCTION

Control applications involving quadrotor unmanned aerial vehicles (UAV) have garnered significant interest in recent years by virtue of their versatility, maneuverability, and ease of use. Quadrotors are a practical solution for a wide array of tasks, including search and rescue, area mapping, and surveillance. The high degree of nonlinearity, state coupling, and general model uncertainty in the quadrotor dynamics create significant challenges in quadrotor control design. As a result, a plethora of research literature exists, which address one or more of these inherent challenges. However, there remains a need for detailed control design and rigorous performance analysis, which formally incorporate the multiple practical limitations inherent in quadrotor control implementation.

One of the most fundamental objectives in quadrotor control applications is that of autonomous trajectory tracking. Tracking control of quadrotors is addressed in [1–10]. In [3], a full experimental treatment of aerial robots is investigated, along with an innovative means of identifying the necessary inverse kinematics. A fuzzy logic approach can be seen in [5], comparing type-1 and type-2 neural networks in terms of performance on a quadrotor system subjected to real-time disturbance experiments. Also noteworthy is [4], which achieves the task of landing a quadrotor upon a moving platform autonomously, making use of only relative position measurements. The task in [4] is divided into three different phases defined in terms of a virtual target point and a safety radius sphere. Quadrotor control applications similar to the aforementioned can often necessitate the design of innovative control algorithms, which address specific challenges inherent in practical control implementation.

In addition to practical implementation challenges, uncertainty in the mathematical models for quadrotor dynamic systems is an unavoidable challenge that must be addressed for reliable control implementation. The task of designing robust control systems for quadrotors is investigated in [11–22, 24]. By virtue of the disturbance rejection capability of sliding mode control (SMC), a SMC method is amalgamated with a backstepping-based design approach to obtain position tracking for a quadrotor in [11]. A global coordinate approach is proposed in [13] to obtain robust attitude tracking of a rigid body in the special orthogonal group in three dimensions (i.e., $SO(3)$). A quadrotor UAV is considered in [17], which makes use of visual targets to estimate translational velocity measurements without the requirement for GPS measurements. The challenges of model uncertainty and actuation time delay due to the use of digital components are addressed in [14, 15]. A distributed formation control algorithm for multiple quadrotor aircraft is presented in [23]. Because the potential sources of uncertainty, disturbances, sensor

Manuscript received February 26, 2018; revised May 15, 2018; accepted June 26, 2018. Recommended by Associate Editor Shihua Li under the direction of Editor Myo Taeg Lim.

Derek Hoffman, Muhammad Rehan, and William MacKunis are with the Department of Physical Sciences, Embry-Riddle Aeronautical University, Daytona Beach, FL 32114, USA (e-mails: {hoffmad2, rehanm}@my.erau.edu, mackuniw@erau.edu). Mahmut Reyhanoglu is with the Department of Engineering, University of North Carolina at Asheville, Asheville, NC 28804, USA (e-mail: reyhanoglu@unca.edu).
* Corresponding author.

measurement limitations, and physical actuator limits are so numerous and varied, there remain many open problems in the design of quadrotor control systems, which are proven to effectively compensate for these unavoidable challenges.

The contribution of this paper is the design and stability analysis of a quaternion-based robust nonlinear attitude tracking controller capable of addressing the uncertainties present in a 3-DOF experimental quadrotor hover system test bed. The use of quaternions is motivated by the desire to reduce the computational burden and eliminate singularities in quadrotor aerial vehicle attitude control applications, where angular velocity measurements are directly available using onboard rate gyros. Also formally addressed in the proposed design are the input voltage constraints inherent in the actuators (i.e, propeller motors). In addition, the proposed control method is shown to compensate for input-multiplicative parametric uncertainty in the dynamic model, which results from unknown drag and friction coefficients in the propeller dynamic model. To avoid excessive computational burden, feed-forward constant estimates of the input-multiplicative uncertainty are implemented, eliminating the need for time-varying parameter adaptation laws. Replacing the conventional (and high-gain demanding) sliding mode observer, a bank of dynamical filters is employed to synthesize velocity estimates for the closed-loop system, so that only position-encoder measurements are required for feedback. A rigorous Lyapunov-based stability analysis is utilized to prove that the closed-loop system achieves asymptotic trajectory tracking in the presence of the aforementioned model uncertainty and practical limitations. Further, a rigorous analysis is provided that determines the sufficient conditions on the control gain selection, within which the input-multiplicative parametric uncertainty can be compensated. Simulation and experimental results are provided to demonstrate the performance of the proposed attitude tracking control law on the Quanser 3-DOF hover system test bed. To the best of the authors' knowledge, this is the first hover system tracking control result that provides a rigorous stability analysis to quantify the range of input-multiplicative parametric uncertainty within which the closed-loop system can be proven to remain asymptotically stable using only angular position measurements for feedback.

The paper is organized as follows: Section 2 describes the mathematical model for the hover system dynamics and kinematics, which are used to develop the control design. Section 3 provides a mathematical description of the tracking control objective using the quaternion kinematic model. Section 4 presents detailed derivations of the control system design and the closed-loop tracking error dynamics. Section 5 provides a detailed Lyapunov-based stability analysis of the closed-loop system. Sections 6 and 7 present numerical simulation and experimental results, respectively, of the proposed control method using the Quanser 3-DOF hover system test bed. Concluding remarks are given in Section 8.

2. MATHEMATICAL MODEL

In this section, the mathematical model for the 3-DOF rotational motion of the quadrotor hover system test bed is presented. In addition to the basic dynamic equations, the dynamic model incorporates the parametric uncertainty and voltage input constraints that are inherent in the hover system. The formal inclusion of these practical considerations in the dynamic model is a key feature, which enables us to design and rigorously analyze a control law that addresses these realistic implementation challenges.

2.1. Dynamic equations

The dynamics of the quadrotor system being considered in this paper can be described using Euler's equations for rigid-body rotation as [25]

$$J\dot{\omega} = -\omega^{\times} J\omega + \tau. \tag{1}$$

In (1), $\omega(t) \triangleq \left[\begin{array}{ccc} \omega_x(t) & \omega_y(t) & \omega_z(t) \end{array}\right]^T \in \mathbb{R}^3$ is the angular velocity of the quadrotor expressed in the body-fixed frame, and $J \in \mathbb{R}^{3\times 3}$ denotes the positive-definite, symmetric inertia matrix. Also in (1), $\zeta^{\times}$, $\forall\ \zeta \in \mathbb{R}^3$, denotes the standard skew-symmetric matrix equivalent to the vector cross-product operation, and $\tau(t) \triangleq \left[\begin{array}{ccc} \tau_x(t) & \tau_y(t) & \tau_z(t) \end{array}\right]^T \in \mathbb{R}^3$ is the generalized torque expressed in the body-fixed frame.

2.1.1 Uncertain electromechanical actuator model

The generalized torque $\tau(t)$ is generated by the combined forces F_i, for $i = 1,...,4$, generated by the propellers onboard the quadrotor hover system. These forces are, in turn, generated by the input voltages V_i, for $i = 1,...,4$, applied to the propellers. Mathematically, the generalized torque can be expressed in terms of the input voltages as

$$\tau \triangleq \left[\begin{array}{c} \tau_x(t) \\ \tau_y(t) \\ \tau_z(t) \end{array}\right] = \left[\begin{array}{c} blK_v^2\left(V_4^2 - V_2^2\right) + J_r\omega_y\Omega_r \\ blK_v^2\left(V_3^2 - V_1^2\right) - J_r\omega_x\Omega_r \\ dK_v^2\left(V_1^2 - V_2^2 + V_3^2 - V_4^2\right) \end{array}\right], \tag{2}$$

where $\Omega_r = K_v(V_1 - V_2 + V_3 - V_4)$ denotes the overall residual angular speed of the propellers. The gyroscopic terms containing Ω_r in (2) manifest themselves as disturbances in the dynamic model, and compensation for these disturbances will be addressed in the subsequent analysis. In (2), $b, d \in \mathbb{R}^+$ denote uncertain thrust and drag coefficients; $l \in \mathbb{R}^+$ is the uncertain distance from the pivot to the motor, $K_v \in \mathbb{R}^+$ denotes an uncertain voltage transformation constant; and $J_r \in \mathbb{R}^+$ is the uncertain rotor inertia (cf. [26]).

To compensate for the parametric uncertainty in the torque model in (2), an auxiliary (virtual) voltage control

signal $u(t) \in \mathbb{R}^3$ is defined via the parameterization

$$Bu = \begin{bmatrix} blK_v^2\left(V_4^2 - V_2^2\right) \\ blK_v^2\left(V_3^2 - V_1^2\right) \\ dK_v^2\left(V_1^2 - V_2^2 + V_3^2 - V_4^2\right) \end{bmatrix}. \tag{3}$$

In (3), the uncertain matrix $B \in \mathbb{R}^{3\times 3}$ and the virtual control input $u(t) \triangleq [u_1(t),\ u_2(t),\ u_3(t)]^T$ are explicitly defined as

$$B \triangleq \begin{bmatrix} blK_v^2 & 0 & 0 \\ 0 & blK_v^2 & 0 \\ 0 & 0 & dK_v^2 \end{bmatrix}, \tag{4}$$

and

$$u = \begin{bmatrix} u_1 \\ u_2 \\ u_3 \end{bmatrix} = \begin{bmatrix} V_4^2 - V_2^2 \\ V_3^2 - V_1^2 \\ V_1^2 - V_2^2 + V_3^2 - V_4^2 \end{bmatrix}. \tag{5}$$

Remark 1 (Input voltage computation)**:** The definition of the virtual control input $u(t)$ in (3) and (5) is motivated by the desire to simplify the control design. In the subsequent analysis, the control law will be designed in terms of the virtual inputs $u_i(t)$, for $i = 1,2,3$; and in experimental implementation, the virtual inputs are transformed to non-negative input voltages by solving (5) for $V_i^2(t)$, for $i = 1,...,4$. For the hover system considered in this paper, the input voltages are required to satisfy $V_i \geq V_b$, $i = 1,\ldots,4$, where $V_b \geq 0$ denotes a bias voltage. We solve (5) for input voltages in terms of the bias voltage and virtual inputs as follows [26]:

$$\begin{aligned} V_2^2 &= \max\left[-\min(u_1,0), -\min(u_2,0) - \hat{u}\right] + V_b^2, \\ V_1^2 &= V_2^2 + \hat{u}, \\ V_3^2 &= V_1^2 + u_2, \\ V_4^2 &= V_2^2 + u_1, \end{aligned} \tag{6}$$

where $\hat{u} := \frac{1}{2}(u_1 - u_2 + u_3)$.

Note that by adding the squared bias voltage V_b^2 to V_2^2, the bias voltage is essentially added to all input voltages. The above solution guarantees that $V_i \geq V_b$, $i = 1,\ldots,4$.

2.2. Kinematic model

The rotational kinematics of the hover system can be described in terms of the standard quaternion parameterization [25]

$$\dot{q}_v = \frac{1}{2}(q_v^{\times}\omega + q_s\omega), \tag{7}$$

$$\dot{q}_s = -\frac{1}{2}q_v^T\omega, \tag{8}$$

where $q_v(t) \in \mathbb{R}^3$ represents the quaternion vector component, and $q_s(t) \in \mathbb{R}$ denotes the scalar component. The quaternion vector can be expressed in the compact form $q(t) \triangleq \{q_v(t), q_s(t)\} \in \mathbb{R}^3 \times \mathbb{R}$, which is subject to the constraint $q_v^T q_v + q_s^2 = 1$.

In the following analysis, the desired unit quaternion $q_d(t) \triangleq \{q_{vd}(t), q_{sd}(t)\} \in \mathbb{R}^3 \times \mathbb{R}$ represents the orientation of the desired body-fixed frame with respect to the fixed inertial frame. Standard quaternion kinematics can be used to show that rotation matrices $R(q_v, q_s) \in SO(3)$ and $R_d(q_{vd}, q_{sd}) \in SO(3)$ can be developed, which bring the inertial frame to the actual and desired frames, respectively.

3. CONTROL OBJECTIVE

The control objective is to force the hover system actual body-fixed frame to track the desired frame. To quantify this objective, an rotational error matrix $\tilde{R}(e_v, e_s) \in \mathbb{R}^{3\times 3}$ is defined as

$$\tilde{R} \triangleq RR_d^T = (e_s^2 - e_v^T e_v)I_3 + 2e_v e_v^T - 2e_s e_v^{\times}, \tag{9}$$

where $e(t) \triangleq \{e_v(t), e_s(t)\} \in \mathbb{R}^3 \times \mathbb{R}$ is the quaternion error, and I_3 denotes the 3×3 identity matrix. Physically, the rotation matrix $\tilde{R}(e_v, e_s)$ represents the rotation that brings the desired body-fixed frame to the actual frame. Thus, the angular velocity error between the actual and desired frames as expressed in the actual body-fixed frame can be obtained as

$$\tilde{\omega} = \omega - \tilde{R}\omega_d. \tag{10}$$

To facilitate the subsequent control design and analysis, an auxiliary error signal, $r(t) \in \mathbb{R}^3$, is defined as

$$r \triangleq \tilde{\omega} + 2\alpha e_v + e_f, \tag{11}$$

where $\alpha \in \mathbb{R}^{3\times 3}$ is a constant, diagonal, positive definite control gain matrix, and $e_f(t) \in \mathbb{R}^3$ is a subsequently defined auxiliary error signal. Note that (11) can be used to express the angular velocity error as

$$\tilde{\omega} = r - 2\alpha e_v - e_f. \tag{12}$$

By using (10), the quaternion error kinematics can be expressed as

$$\dot{e}_v = \frac{1}{2}W(e)\tilde{\omega}, \tag{13}$$

$$\dot{e}_s = -\frac{1}{2}e_v^T\tilde{\omega}, \tag{14}$$

where the auxiliary matrix $W(e) \in \mathbb{R}^{3\times 3}$ is defined as

$$W(e) = e_v^{\times} + e_s I_3. \tag{15}$$

Based on the aforementioned variable definitions, it can be shown that the quaternion error satisfies the constraint [25]

$$e_v^T e_v + e_s^2 = 1. \tag{16}$$

Based on (9) and (16), the control objective can be stated mathematically as $\|e_v(t)\| \to 0$, which in turn implies that $\tilde{R}(e_v, e_s) \to I_3$.

Assumption 1: The subsequent error system development and stability analysis is based on the standard assumption that the desired trajectory remains bounded in the sense that $\omega_d(t)$, $\dot{\omega}_d(t) \in \mathcal{L}_\infty$ and $q_d(t)$, $\dot{q}_d(t)$, $\ddot{q}_d(t) \in \mathcal{L}_\infty$ throughout closed-loop controller operation.

4. CONTROL DEVELOPMENT

The contribution in this paper is a rigorous error system development and robust nonlinear control design, which are proven to achieve attitude control for a quadrotor hover system test bed in the presence of input-multiplicative parametric uncertainty, unmodeled dynamics, and control voltage input constraints. Moreover, to address the practical implementation consideration that only angular position encoders are available for feedback, an output feedback control strategy is employed, which is shown to achieve asymptotic attitude regulation using only the available measurements of position.

4.1. Open-loop error dynamics

The auxiliary error signal $e_f(t)$ introduced in (11) is an output of a bank of dynamic filters defined as [27]

$$\dot{p} = -(k+2\alpha)p - \eta + 2(k+\alpha)^2 e_v + e_v, \tag{17}$$

$$\dot{\eta} = p - \alpha\eta - 2(k+\alpha)e_v, \tag{18}$$

$$e_f = p - 2(k+\alpha)e_v. \tag{19}$$

In (17)-(19), $k \in \mathbb{R}^{3\times 3}$ denote a constant, diagonal, positive definite control gain matrix; $\eta(t) \in \mathbb{R}^3$ denotes another output of the filter; and $p(t) \in \mathbb{R}^3$ is an internal filter variable.

After taking the time derivative of (19) and using (12), (13), and (17), $\dot{e}_f(t)$ can be expressed as

$$\dot{e}_f = -\alpha e_f - \eta + e_v - (k+\alpha)r - (k+\alpha)\Delta(e)\tilde{\omega}, \tag{20}$$

where $\Delta(e) \in \mathbb{R}^{3\times 3}$ is defined as

$$\Delta(e) = W(e) - I_3. \tag{21}$$

The expression in (20) will be used in the subsequent stability analysis.

Assumption 2: It is assumed that the matrix mismatch term $\Delta(e)$ satisfies

$$\|\Delta(e)\|_{i\infty} \leq \varepsilon < 1, \tag{22}$$

where $\varepsilon \in \mathbb{R}^+$ is a known bounding constant, and $\|\cdot\|_{i\infty}$ denotes the induced infinity norm of a matrix. The bounding condition in (22) can be interpreted as a limit on the region of convergence of the proposed control law. This can be practically viewed as a control design trade-off that is required to prove asymptotic attitude regulation in the presence of the input-multiplicative parametric uncertainty that is inherent in the hover system test bed. Preliminary results show that Assumption 2 is mild in the sense that the proposed control law achieves asymptotic attitude regulation over a wide operational range.

After taking the time derivative of $r(t)$ in (11) and premultiplying the result by J, the open-loop error dynamics are obtained as

$$J\dot{r} = J\dot{\omega} + J\tilde{\omega}^{\times}\tilde{R}\omega_d - J\tilde{R}\dot{\omega}_d + 2J\alpha\dot{e}_v + \dot{e}_f, \tag{23}$$

where the fact that $\dot{\tilde{R}} = -\tilde{\omega}^{\times}\tilde{R}$ was utilized. By substituting the dynamic model (1) into (23), the open-loop system can be expressed as

$$\begin{aligned} J\dot{r} = &-\omega^{\times}J\omega + Bu + J\tilde{\omega}^{\times}\tilde{R}\omega_d - J\tilde{R}\dot{\omega}_d \\ &+ J\alpha W(e)\tilde{\omega} - \alpha e_f - \eta + e_v - (k+\alpha)r \\ &- (k+\alpha)\Delta(e)\tilde{\omega} + \chi(\omega), \end{aligned} \tag{24}$$

where (2), (3), (13), and (20) were utilized. In (24), the auxiliary term $\chi(\omega) \in \mathbb{R}^3$ contains gyroscopic disturbances as

$$\chi(\omega) \triangleq \begin{bmatrix} J_r\omega_y\Omega_r \\ -J_r\omega_x\Omega_r \\ 0 \end{bmatrix}. \tag{25}$$

To facilitate the subsequent nonlinear control design and stability analysis, the open-loop error system (24) is rewritten as

$$J\dot{r} = \tilde{N} + Bu + \Lambda\alpha e_f - \Lambda e_v - (k+\alpha)r, \tag{26}$$

where $\Lambda \in \mathbb{R}^{3\times 3}$ is a subsequently defined uncertain auxiliary matrix, and the unmeasurable auxiliary term $\tilde{N}(t) \in \mathbb{R}^3$ is explicitly defined as

$$\begin{aligned} \tilde{N} \triangleq &-\omega^{\times}J\omega + J\tilde{\omega}^{\times}\tilde{R}\omega_d - J\tilde{R}\dot{\omega}_d + J\alpha W(e)\tilde{\omega} \\ &- (\Lambda+\alpha)e_f - \eta + e_v + \Lambda e_v - (k+\alpha)\Delta(e)\tilde{\omega} \\ &+ \chi(\omega). \end{aligned} \tag{27}$$

The motivation for the grouping of terms in (27) is based on the subsequent stability analysis and the fact that the following upper bound can be developed:

$$\left\|\tilde{N}\right\| \leq \rho(\|z\|)\|z\|, \tag{28}$$

where $\rho(\cdot) \in \mathbb{R}$ is a positive, globally invertible nondecreasing function; and $z(t) \in \mathbb{R}^{12}$ is defined as

$$z(t) \triangleq \begin{bmatrix} e_v^T(t) & e_f^T(t) & r^T(t) & \eta^T(t) \end{bmatrix}^T. \tag{29}$$

4.2. Closed-loop error system

Based on the open-loop error system in (26) and the subsequent stability analysis, the control input term $u(t)$ is designed as

$$u(t) = \hat{B}^{-1}(ke_f(t)), \tag{30}$$

where k is a control gain introduced in (17)-(19). In (30), $\hat{B} \in \mathbb{R}^{3\times 3}$ is a feedforward matrix containing constant, 'best guess' estimates $\hat{b}$, $\hat{d}$, $\hat{l}$, $\hat{K}_v \in \mathbb{R}^+$ of the uncertain parameters b, d, l, K_v in (3). Specifically, $\hat{B}$ is defined as

$$\hat{B} \triangleq \begin{bmatrix} \hat{b}\hat{l}\hat{K}_v^2 & 0 & 0 \\ 0 & \hat{b}\hat{l}\hat{K}_v^2 & 0 \\ 0 & 0 & \hat{d}\hat{K}_v^2 \end{bmatrix}. \tag{31}$$

After substituting (30) into (26), the closed-loop error system is obtained as

$$J\dot{r} = \tilde{N} + \Lambda(ke_f) + \Lambda\alpha e_f - \Lambda e_v - (k+\alpha) r, \tag{32}$$

where the uncertain constant mismatch matrix $\Lambda \in \mathbb{R}^{3\times 3}$ is defined as

$$\Lambda \triangleq B\hat{B}^{-1}. \tag{33}$$

Property 1: Since the symmetric matrix Λ is positive definite, its inverse Λ^{-1} is positive definite and symmetric.

Remark 2 (Use of constant estimates)**:** The use of constant parameter estimates in the control law (30) is motivated by the desire to reduce the computational burden in the closed-loop system. The experimental results demonstrate that the proposed control law achieves reliable attitude control under significant parametric uncertainty.

By leveraging Property 1, the closed-loop error system in (32) can be rewritten as

$$\Lambda^{-1}J\dot{r} = \tilde{N}_1 + (k+\alpha) e_f - e_v - \Lambda^{-1}(k+\alpha) r, \tag{34}$$

where $\tilde{N}_1 \in \mathbb{R}^3$ is defined as

$$\tilde{N}_1 \triangleq \Lambda^{-1}\tilde{N}. \tag{35}$$

Based on Property 1 and Inequality (28), the auxiliary term $\tilde{N}_1(t)$ satisfies

$$\left\|\tilde{N}_1\right\| \leq \rho_1(\|z\|)\|z\|, \tag{36}$$

where $\rho_1(\cdot) \in \mathbb{R}$ is a positive, globally invertible nondecreasing function.

5. STABILITY ANALYSIS

Theorem 1: The robust nonlinear output feedback control law given in (17)-(19), (30), and (31) ensures that all system signals remain bounded throughout closed-loop controller operation and ensures asymptotic attitude regulation in the sense that

$$\|e_v(t)\| \to 0 \qquad \text{as} \qquad t \to \infty \tag{37}$$

provided (22) is satisfied and the control gain k introduced in (17)-(19) is selected to satisfy the subsequently defined sufficient condition.

Proof: Consider the nonnegative function $V(t)$ defined as

$$V = e_v^T e_v + (1-e_s)^2 + \frac{1}{2}\left(e_f^T e_f + r^T\Lambda^{-1}Jr + \eta^T\eta\right). \tag{38}$$

After taking the time derivative of (38) and utilizing (13), (14), (18), (20), and (34) and cancelling common terms $\dot{V}(t)$ can be upper bounded as

$$\dot{V} \leq -\lambda_\alpha\|z\|^2 + \varepsilon(\lambda_k+\lambda_\alpha)\|z\|^2 - \lambda_{\Lambda k}\left(\|r\|^2 - \frac{\rho_1(\|z\|)}{\lambda_{\Lambda k}}\|z\|\|r\|\right), \tag{39}$$

where Inequality (22) of Assumption 2 was utilized. In (39), $\lambda_\alpha \triangleq \lambda_{\min}(\alpha)$, $\lambda_k \triangleq \lambda_{\min}(k)$, and $\lambda_{\Lambda k} \triangleq \lambda_{\min}\left(\Lambda^{-1}k\right)$, with $\lambda_{\min}(\cdot)$ denoting the minimum eigenvalue of the argument. After completing the squares in the parenthetic terms in (39), the upper bound in (39) can be expressed as

$$\dot{V} \leq -\left(\lambda_\alpha - \left(\frac{\rho_1^2(\|z\|)}{4\lambda_{\Lambda k}} + \varepsilon(\lambda_k+\lambda_\alpha)\right)\right)\|z\|^2. \tag{40}$$

Inequality (40) can be expressed as

$$\dot{V} \leq -c_0\|z\|^2 \tag{41}$$

where $c_0 \in \mathbb{R}^+$ denotes a bounding constant that is defined over the domain $\mathcal{D}$ given by

$$\mathcal{D} \triangleq \left\{z \in \mathbb{R}^{12} : \|z\| < \rho_1^{-1}\left(\sqrt{4\lambda_{\Lambda k}\lambda_\alpha - \varepsilon(\lambda_k+\lambda_\alpha)}\right)\right\}. \tag{42}$$

The existence of the region of convergence can be ensured provided the control gain matrices k and α are selected to satisfy the sufficient condition

$$\lambda_{\min}\left(\Lambda^{-1}k\right)\frac{\lambda_{\min}(\alpha)}{\lambda_{\max}(k)+\lambda_{\max}(\alpha)} > \frac{\varepsilon}{4}, \tag{43}$$

where Λ is introduced in (33), and ε is introduced in (22). The control gain matrices k and α can be selected to satisfy the sufficient condition in (43), provided Assumption 2 is satisfied.

Remark 3 (Sufficient gain conditions under uncertainty)**:** The expression in (43) can be physically interpreted as the maximum deviation between the actual and estimated input gain matrices B and $\hat{B}$ that can be tolerated for the proposed closed-loop system to achieve asymptotic attitude regulation. It should be noted that Inequality (43) represents a *sufficient*, *not necessary*, condition. The subsequent experimental results demonstrate that the closed-loop system achieves asymptotic attitude regulation in the presence of significant input-multiplicative parametric uncertainty.

Based on (38) and (41), it follows that $z(t) \in \mathcal{L}_\infty$ in $\mathcal{D}$, hence $e_v(t)$, $e_s(t)$, $e_f(t)$, $r(t)$, $\eta(t) \in \mathcal{L}_\infty$ in $\mathcal{D}$. Given

that $r(t), e_v(t), e_f(t) \in \mathcal{L}_\infty$, (12) can be used to show that $\tilde{\omega}(t) \in \mathcal{L}_\infty$ in $\mathcal{D}$; and Assumption 1 can be used along with (10) to show that $\omega(t) \in \mathcal{L}_\infty$ in $\mathcal{D}$. Since $\tilde{\omega}(t), e_v(t), e_s(t) \in \mathcal{L}_\infty$, Equations (13) and (14) can be used to show that $\dot{e}_v(t), \dot{e}_s(t) \in \mathcal{L}_\infty$ in $\mathcal{D}$. Given that $e_v(t), e_f(t), r(t), \tilde{\omega}(t) \in \mathcal{L}_\infty$, (20) can be used to show that $\dot{e}_f(t) \in \mathcal{L}_\infty$ in $\mathcal{D}$. Since $\eta(t), e_v(t) \in \mathcal{L}_\infty$, Theorem 1.1 of [28] can be used with (17) to prove that $p(t), \dot{p}(t) \in \mathcal{L}_\infty$ in $\mathcal{D}$. Given that $p(t), \eta(t), e_v(t) \in \mathcal{L}_\infty$, it follows from (18) that $\dot{\eta}(t) \in \mathcal{L}_\infty$ in $\mathcal{D}$. Since $e_f(t) \in \mathcal{L}_\infty$, (30) can be used to show that the control input $u(t) \in \mathcal{L}_\infty$ in $\mathcal{D}$. Given that $e_v(t), e_s(t), e_f(t), r(t), \eta(t), \omega(t), \tilde{\omega}(t), u(t) \in \mathcal{L}_\infty$, the expressions in (24) and (25) can be utilized along with Assumption 1 to show that $\dot{r}(t) \in \mathcal{L}_\infty$ in $\mathcal{D}$. Since $\dot{e}_v(t), \dot{e}_f(t), \dot{r}(t), \dot{\eta}(t) \in \mathcal{L}_\infty$, the definition in (29) can be used to show that $\dot{z}(t) \in \mathcal{L}_\infty$ in $\mathcal{D}$; hence, $z(t)$ is uniformly continuous in $\mathcal{D}$. The expressions in (38) and (41) can then be used to prove that $z(t) \in \mathcal{L}_\infty \cap \mathcal{L}_2$ in $\mathcal{D}$. Barbalat's lemma can now be invoked to prove that [29]

$$\|z(t)\|^2 \to 0 \quad \text{as} \quad t \to \infty \quad \forall\, z(0) \in \mathcal{D}. \tag{44}$$

Hence, (44) can be used along with (29) to prove that

$$\|e_v(t)\| \to 0 \quad \text{as} \quad t \to \infty \quad \forall\, z(0) \in \mathcal{D}. \tag{45}$$

Since the region of convergence depends on the initial conditions, it follows that the result is **locally asymptotically stable (LAS)**, where the radius of convergence has been shown to depend on the degree of parametric uncertainty in the input gain matrix B (see (42)).

6. NUMERICAL SIMULATION RESULTS

To validate the proposed hover system control method, a numerical simulation was created using Matlab/Simulink. The model applies the dynamics outlined in (1) and (3), with control input conversion to voltage (5) to address control saturation behavior. The dynamic bank of filters defined in (17)-(19) fulfills its role of providing velocity estimates for the control input described in (30) and (31). For the quadrotor dynamics, the nominal parameter values shown in Table 1 are utilized to obtain the moment of inertia matrix for the plant model. The nominal parameters are used to define the plant model only. They are assumed to be unknown and are not used in the control law. The proposed robust control design compensates for the uncertainty.

The simulation results presented here correspond to control gains

$$\alpha = \text{diag}\{2.7, 3, 3\}, \; k = \text{diag}\{4.2, 0.7, 0.7\},$$

while the feed-forward estimate matrix makes use of the estimated parameters in Table I applied to (30). In all three terms, the values provided were the result of combining dynamical insight with desired performance such as settling time and required voltage.

Table 1. Nominal and estimated input-multiplicative parameters used in the experiment.

Parameter		Value
Thrust coef. *Nominal*	b	3.935×10^{-6} $\frac{\text{N}}{\text{V}}$
Estimate	$\hat{b}$	4.317×10^{-5} $\frac{\text{N}}{\text{V}}$
Drag coef. *Nominal*	d	1.193×10^{-7} $\frac{\text{Nm}}{\text{V}}$
Estimate	$\hat{d}$	3.054×10^{-6} $\frac{\text{Nm}}{\text{V}}$
Trans. const. *Nominal*	K_v	54.945 $\frac{\text{rad}}{\text{sV}}$
Estimate	$\hat{K}_v$	34.341 $\frac{\text{rad}}{\text{sV}}$
Pivot to motor *Nominal*	l	0.197 m
Estimate	$\hat{l}$	0.276 m

It must be noted that the Quanser test bed reads angular position input in Euler angle notation, hence the simulation must be converted in order to have a direct comparison. While additional coding is implemented to ensure that the unit quaternion constraint is always satisfied for the simulation application, the provided range of initial displacements reside in the first quadrant and thus do not see ambiguity in unit quaternion transformation.

In order to clearly show the wide range of allowable initial conditions provided by the feed-forward estimate paradigm, a Monte Carlo-esque simulation scheme is provided, that investigates a family of initial angle conditions spanning from 5 to 25 degrees with an increment of 5 degrees for all three Euler angles. The remaining initial conditions of angular velocities and filter starting points were set to 0. Two separate goals of roll $\phi(t)$ and pitch $\theta(t)$ tracking of a desired sinusoidal trajectory (i.e., $\phi_d(t)$ and $\theta_d(t)$) were demonstrated, where the desired trajectory is defined as

$$\phi_d(t) = \theta_d(t) = 10\sin(0.5t). \tag{46}$$

The desired trajectory in (46) is expressed in degrees, and the desired yaw angle and the remaining Euler angle in both cases are defined as 0, without loss of generality. In order to demonstrate a realistic scenario, a 10 percent noise factor was added to the quaternion position measurement. The results of the control algorithm described can be seen in Figs. 1-4. Specifically, Figs. 1 and 3 demonstrate effective tracking of the desired commands within 4 seconds for a wide range of initial angular positions, while Figs. 2 and 4 prove that the saturation voltage constraint is respected, and that none of the provided scenarios exhibit control saturation. In short, the feed-forward estimate approach in conjunction with the bank of dynamic filters can be proven to be effective for a wide performance envelope.

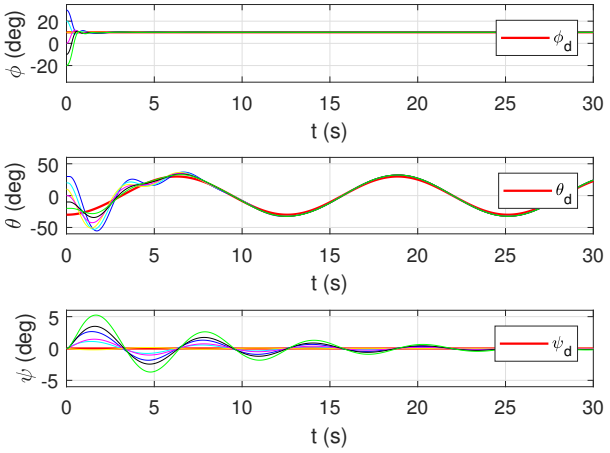

Fig. 1. Monte Carlo simulation results (pitch tracking): the roll, pitch, and yaw displacements during closed-loop controller operation of the simulated hover system model.

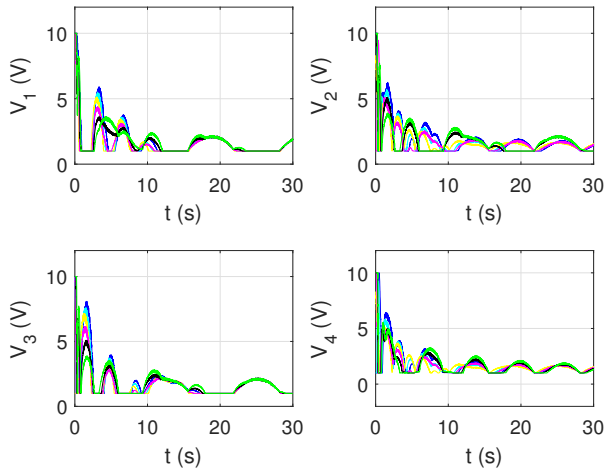

Fig. 2. Monte Carlo simulation results (pitch tracking): voltages $V_1(t)$, $V_2(t)$, $V_3(t)$, and $V_4(t)$ [V] applied to the four propellers during closed-loop attitude controller operation.

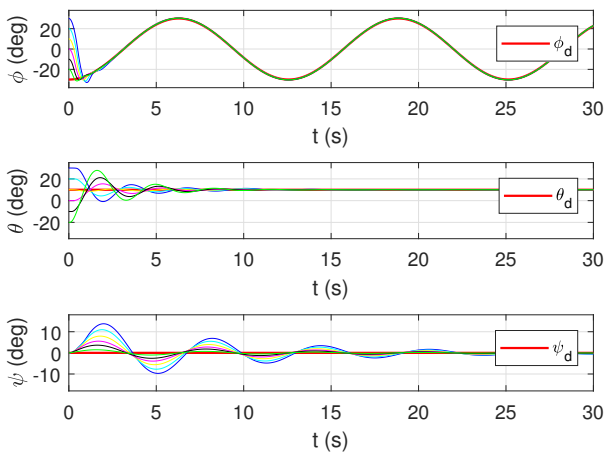

Fig. 3. Monte Carlo simulation results (roll tracking): the roll, pitch, and yaw displacements during closed-loop controller operation of the simulated hover system model.

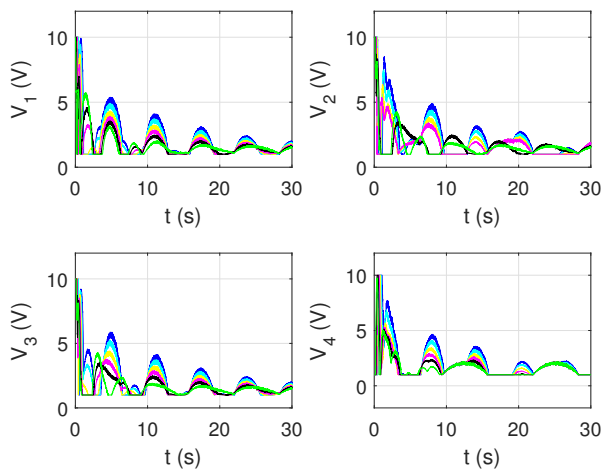

Fig. 4. Monte Carlo simulation results (roll tracking): voltages $V_1(t)$, $V_2(t)$, $V_3(t)$, and $V_4(t)$ [V] applied to the four propellers during closed-loop attitude controller operation.

7. EXPERIMENTAL RESULTS

To demonstrate the performance of the proposed attitude tracking technique, an experiment was performed using the Quanser 3-DOF hover system test bed (see Fig. 5). The test bed consists of a quadrotor helicopter system mounted at the center of gravity on an air bearing joint, such that the hover system is free to rotate in all three rotational degrees of freedom. Roll, pitch, and yaw encoders (with a resolution of 8192 counts per revolution) are used for angular position measurements. The control law in the experiment uses the bank of filters in (17)-(19) along with the control law in (30) and (31). The control law incorporates the estimated parameter values in Table 1. It should be noted that the nominal values of the inertia parameters of the test bed are assumed to be unknown and are not used in the control law.

The initial conditions of Euler angles, angular velocities and filter starting points were set to 0. Two separate goals of roll $\phi(t)$ and pitch $\theta(t)$ tracking of a desired sinusoidal trajectory (i.e., $\phi_d(t)$ and $\theta_d(t)$) were demonstrated, where the desired trajectory is defined as

$$\phi_d(t) = \theta_d(t) = 10\sin(0.5t). \tag{47}$$

The desired trajectory in (47) is expressed in degrees, and the desired yaw angle is defined as 0, with the remaining Euler angle in both cases following a step command of

Fig. 5. Quadrotor hover system (Quanser.com).

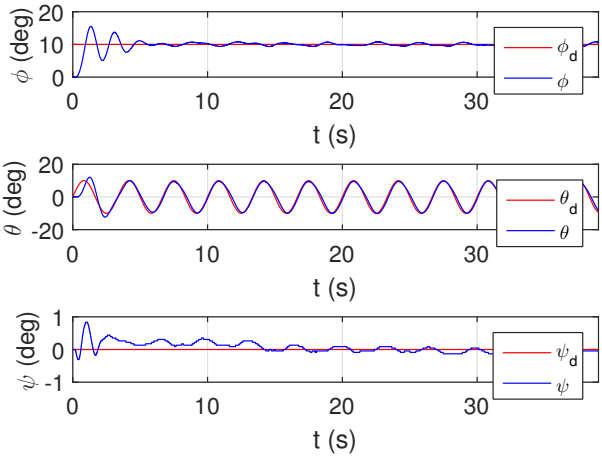

Fig. 6. Experimental results (pitch tracking): time response of the roll, pitch, and yaw displacements during closed-loop controller operation of the simulated hover system model.

10 degrees, without loss of generality. Figs. 6-9 summarize the experimental results achieved using the proposed output feedback control law with control gains selected as

$$\alpha = diag\{2.7,3,3\}\,,\; k = diag\{4.2,0.7,0.7\}\,.$$

To ease the interpretation of the experimental results, the closed-loop response in Figs. 6 and 8 is provided in terms of roll, pitch, and yaw displacements.

Moreover, Figs. 7 and 9 show that the commanded control signals remain within reasonable voltage limits throughout closed-loop controller operation. The experimental results further demonstrate the capability of the proposed control method to stabilize the hover system test bed in the presence of significant uncertainty in the physical parameters inherent in the test bed (see Table 1).

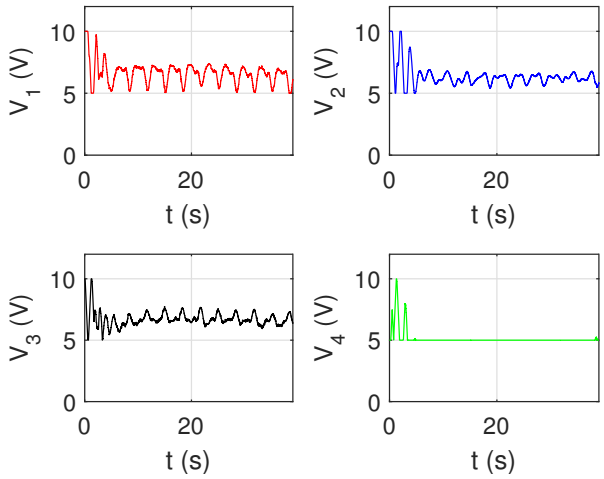

Fig. 7. Experimental results (pitch tracking): voltages $V_1(t)$, $V_2(t)$, $V_3(t)$, and $V_4(t)$ [V] applied to the four propellers during closed-loop attitude controller operation.

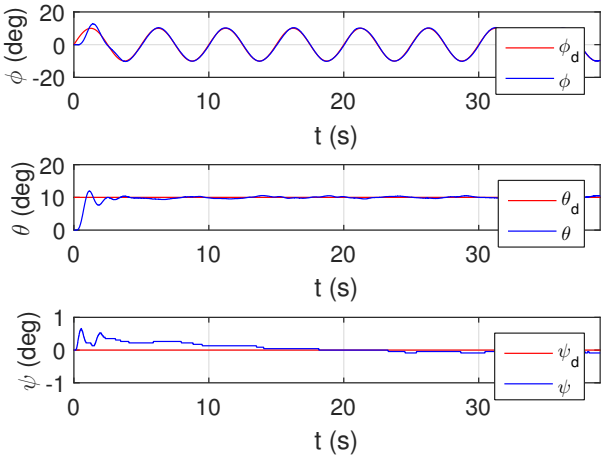

Fig. 8. Experimental results (roll tracking): time response of the roll, pitch, and yaw displacements during closed-loop controller operation of the simulated hover system model.

8. CONCLUSIONS

A robust nonlinear output feedback control law, which achieves 3-DOF attitude tracking of a quadrotor hover system test bed, is presented. The proposed control method formally incorporates the practical voltage constraints inherent in the control actuators (i.e., the quadrotor propellers). In addition, the control law is designed to compensate for significant model uncertainty, including input-multiplicative parametric uncertainty in the propellers' dynamic model. To address a practical scenario, where only position encoder measurements are available for feedback, the control method utilizes a bank of dy-

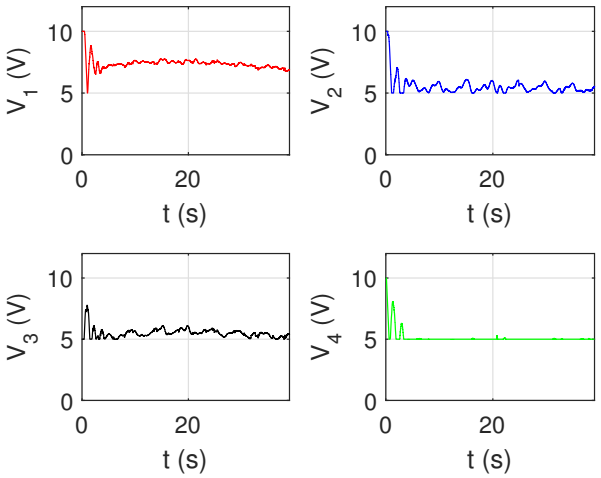

Fig. 9. Experimental results (roll tracking): voltages $V_1(t)$, $V_2(t)$, $V_3(t)$, and $V_4(t)$ [V] applied to the four propellers during closed-loop attitude controller operation.

namic filters, which operates as a velocity estimator in the closed-loop system. A Lyapunov-based stability analysis is presented to prove the theoretical result, where detailed control gain conditions are derived to compensate for parametric input uncertainty. Experimental results are provided to illustrate that the closed-loop system exhibits favorable attitude control performance in the presence of significant input-multiplicative parametric uncertainty, using only position encoder measurements for feedback.

REFERENCES

[1] Y.-C. Choi and H.-S. Ahn, "Nonlinear control of quadrotor for point tracking: actual implementation and experimental tests," *IEEE/ASME Transactions on Mechatronics*, vol. 20, no. 3, pp. 1179-1192, 2015.

[2] M. Faessler, D. Falanga, and D. Scaramuzza, "Thrust mixing, saturation, and body-rate control for accurate aggressive quadrotor flight," *IEEE Robotics and Automation Letters*, vol. 2, no. 2, pp. 476-482, 2017.

[3] M. Fanni and A. Khalifa, "A new 6-DOF quadrotor manipulation system: design, kinematics, dynamics, and control," *IEEE/ASME Transactions on Mechatronics*, vol. 22, no. 3, pp. 1315-1326, 2017.

[4] J. Ghommam and M. Saad, "Autonomous landing of a quadrotor on a moving platform," *IEEE Transactions on Aerospace and Electronic Systems*, vol. 53, no. 3, pp. 1504-1519, 2017.

[5] E. Kayacan and R. Maslim, "Type-2 fuzzy logic trajectory tracking control of quadrotor VTOL aircraft with elliptic membership functions," *IEEE/ASME Transactions on Mechatronics*, vol. 22, no. 1, pp. 339-348, 2017.

[6] M. Reinosa, L. I. Minchala, J. P. Ortiz, D. Astudillo, and D. Verdugo, "Trajectory tracking of a quadrotor using sliding mode control," *IEEE Latin America Transactions*, vol. 16, no. 5, pp. 2157-2166, 2016.

[7] Y. Yu and X. Ding, "A global tracking controller for underactuated aerial vehicles: design, analysis, and experimental tests on quadrotor," *IEEE/ASME Transactions on Mechatronics*, vol. 21, no. 5, pp. 2499-2511, 2016.

[8] B. Zhao, B. Xian, Y. Zhang, and X. Zhang, "Nonlinear robust adaptive tracking control of a quadrotor UAV via immersion and invariance methodology," *IEEE Transactions on Industrial Electronics*, vol. 62, no. 5, pp. 2891-2902, 2015.

[9] Y. Zuo, "Trajectory tracking controller for quadrotors without velocity and angular velocity measurements," *IET Control Theory and Applications*, vol. 11, no. 1, pp. 101-109, 2017.

[10] Z. Zuo, "Trajectory tracking control design with command-filtered compensation for a quadrotor," *IET Control Theory and Applications*, vol. 4, no. 11, pp. 2343-2355, 2010.

[11] F. Chen, R. Jiang, K. Zhang, B. Jiang, and G. Tao, "Robust backstepping sliding mode-control and observer-based fault estimation for a quadrotor UAV, " *IEEE Transactions on Industrial Electronics*, vol. 63, no. 8, pp. 5044-5056, 2016.

[12] S. Islam, P. Liu, and A. E. Saddik, "Robust control of four-rotor unmanned aerial vehicle with disturbance uncertainty," *IEEE Transactions on Industrial Electronics*, vol. 62, no. 3, pp. 1563-1571, 2015.

[13] T. Lee, "Robust adaptive attitude tracking on SO(3) with an application to a quadrotor UAV," *IEEE Transactions on Control Systems Technology*, vol. 21, no. 5, pp. 1924-1930, 2013.

[14] H. Liu, J. Xi, and Y. Zhong, "Robust attitude stabilization for nonlinear quadrotor systems with uncertainties and delays," *IEEE Transactions on Industrial Electronics*, vol. 64, no. 7, pp. 5585-5594, 2017.

[15] H. Liu, W. Zhao, Z. Zuo, and Y. Zhong, "Robust control for quadrotors with multiple time-varying uncertainties and delays," *IEEE Transactions on Industrial Electronics*, vol. 64, no. 2, pp. 1303-1312, 2017.

[16] D. Ma, Y. Xia, T. Li, and K. Chang, "Active disturbance rejection and predictive control strategy for a quadrotor helicopter," *IET Control Theory and Applications*, vol. 10, no. 17, pp. 2213-2222, 2016.

[17] R. Mebarki, V. Lippiello, and B. Siciliano, "Nonlinear visual control of unmanned aerial vehicles in GPS-denied environments," *IEEE Transactions on Robotics*, vol. 31, no. 4, pp. 1004-1017, 2015.

[18] J. P. Ortiz, L. I. Minchala, and M. J. Reinoso, "Nonlinear robust H-Infinity PID controller for the multivariable system quadrotor," *IEEE Latin America Transactions*, vol. 14, no. 3, pp. 1176-1183, 2016.

[19] T. Ryan and H. J. Kim, "LMI-based gain synthesis for simple robust quadrotor control," *IEEE Transactions on Automation Sciences and Engineering*, vol. 10, no. 4, pp. 1173-1178, 2013.

[20] A. C. Satici, H. Poonawala, and M. W. Spong, "Robust optimal control of quadrotor UAVs," *IEEE Access*, vol. 1, no. 1, pp. 79-93, 2013.

[21] A. P. Sandiwan, A. Cahyadi, and S. Herdjunanto, "Robust proportional-derivative control on SO(3) with disturbance compensation for quadrotor UAV," *International Journal of Control, Automation and Systems*, vol. 15, no. 5, pp. 2329-2342, 2017.

[22] A. E. Rodriguez-Mata, I. Gonzalez-Hernandez, J. G. Rangel-Peraza, S. Salazar, and R. L. Leal, "Wind-gust compensation algorithm based on high-gain residual observer to control a quadrotor aircraft: real-time verification task at fixed point," *International Journal of Control, Automation and Systems*, vol. 16, no. 2, pp. 856-866, 2018.

[23] H. Du, W. Zhu, G. Wen, Z. Duan, and J. Lu, "Distributed formation control of multiple quadrotor aircraft based on nonsmooth consensus algorithms," *IEEE Transactions on Cybernetics*, pp. 1-12, 2017.

[24] S. Stebler, W. MacKunis, and M. Reyhanoglu, "Nonlinear output feedback tracking control of a quadrotor UAV in the presence of uncertainty," *Proceedings of International Conference on Control, Automation, Robotics and Vision*, pp. 1-6, 2016.

[25] P. Hughes, *Spacecraft Attitude Dynamics*, Wiley, New York, 1994.

[26] R. Damen, M. Reyhanoglu, W. MacKunis, and J. R. Hervas, "Passivity-based quaternion feedback control of a hover system," *Proceedings of International Conference on Control, Automation and Systems*, pp. 201-206, 2016.

[27] B. Xian, D. M. Dawson, M. S. de Queiroz, and J. Chen, "A continuous asymptotic tracking control strategy for uncertain nonlinear systems," *IEEE Transactions on Automatic Control*, vol. 49, no. 7, pp. 1206–1211, 2004.

[28] D. Dawson, M. Bridges, and Z. Qu, *Nonlinear Control of Robotic Systems for Environmental Waste and Restoration*, Prentice Hall PTR, Englewood Cliffs, New Jersey, 1995.

[29] H. Khalil, *Nonlinear Systems*, Prentice Hall, 2002.

Derek Hoffman received his Ph.D. degree in Engineering Physics from Embry-Riddle Aeronautical University, Daytona Beach, in 2018 with a dissertation focus in nonlinear control of underactuated and constrained systems. Shortly after, he began employment with Raytheon Missile Systems in Tucson, AZ as a senior systems engineer under the Guidance, Navigation, and Control department.

Muhammad Rehan received his Ph.D. degree in Engineering Physics from Embry Riddle Aeronautical University, Daytona Beach, in 2018 with a dissertation focus in dynamics and control of a class of nonholonomic systems. After completing his doctoral studies, he began working as a postdoctoral fellow at the University of Central Florida. His current research focus is on data analytic for energy management systems.

William MacKunis received his Ph.D. degree in 2009 from the Department of Mechanical and Aerospace Engineering at the University of Florida (UF) as a UF Alumni Fellow. After completing his doctoral studies, he was selected as a National Research Council (NRC) Postdoctoral Research Associate at the Air Force Research Laboratory Munitions Directorate at Eglin Air Force Base, where he worked in the Guidance and Navigation Division. In 2010, Dr. MacKunis joined the faculty of Embry-Riddle Aeronautical University in the Department of Physical Sciences, where he is currently an associate professor. His main research is in the development and application of Lyapunov-based control techniques for mechanical and aerospace systems with uncertain nonlinear dynamic models. He is the co-author of two book chapters and over 80 refereed journal articles and conference papers. He is currently or has served as an associate editor for the IEEE Control Systems Society (CSS) Editorial Board and Journal of Control Science and Engineering.

Mahmut Reyhanoglu is presently the Glaxo Wellcome Distinguished Professor of Engineering at the University of North Carolina at Asheville, North Carolina, USA. His major research interests are in the areas of nonlinear dynamical systems and control theory, with particular emphasis on applications to mechatronics and aerospace systems. He has edited 3 books, and authored/co-authored several book chapters and over 130 peer-reviewed journal/proceedings papers. He served on the IEEE Transactions on Automatic Control Editorial Board and on the IEEE Control Systems Society Conference Editorial Board as an Associate Editor. He also served as International Program Committee member for several conferences and as a member of AIAA Guidance, Navigation, and Control Technical Committee. He is currently serving as an editor of International Journal of Aerospace Engineering.